Applied Physics Letters

All-fiber focused beam generator integrated on an optical fiber tip

Cite as: Appl. Phys. Lett. **116**, 241102 (2020); https://doi.org/10.1063/5.0007022
Submitted: 10 March 2020 . Accepted: 04 June 2020 . Published Online: 16 June 2020

Jian Yu, Yi-Ping Wang, Wu Yang, Zhi-Yong Bai, Zhenwei Xie, Zhao Liu, and Chang-Rui Liao

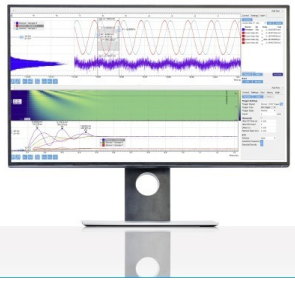

Applied Physics Letters ARTICLE scitation.org/journal/apl

All-fiber focused beam generator integrated on an optical fiber tip

Cite as: Appl. Phys. Lett. **116**, 241102 (2020); doi: 10.1063/5.0007022
Submitted: 10 March 2020 · Accepted: 4 June 2020 ·
Published Online: 16 June 2020

Jian Yu,[1,2] Yi-Ping Wang,[1,2] Wu Yang,[3] Zhi-Yong Bai,[1,2,a)] Zhenwei Xie,[3,a)] Zhao Liu,[1,2] and Chang-Rui Liao[1,2,b)]

AFFILIATIONS

[1]Key Laboratory of Optoelectronic Devices and Systems of Ministry of Education and Guangdong Province, College of Optoelectronic Engineering, Shenzhen University, Shenzhen 518060, China
[2]Guangdong and Hong Kong Joint Research Centre for Optical Fibre Sensors, College of Physics and Optoelectronic Engineering, Shenzhen University, Shenzhen 518060, China
[3]Nanophotonics Research Centre, Shenzhen Key Laboratory of Micro-Scale Optical Information Technology, Institute of Microscale Optoelectronics, Shenzhen University, Shenzhen 518060, China

[a)]**Authors to whom correspondence should be addressed:** baizhiyong@szu.edu.cn and ayst3_1415926@sina.com
[b)]**Present address:** 3688 Nanhai Avenue, Nanshan District, Shenzhen Guangdong 518056, China.

ABSTRACT

We report a compact all-fiber focused vortex beam generator, where a spiral zone plate (SZP) is integrated on the tip of a composite optical fiber microstructure with the femtosecond laser two-photon polymerization. The experimental characteristics of the beam produced from the focused vortex beam generators, such as the focal length, focal spot diameter, and vortex topological charge, are in excellent agreement with the results from finite-difference time-domain simulations. Adjusting the design parameters of the SZP integrated on the fiber tip, we can realize the precise manipulation of the generator's output light field. Since the intrinsic high divergence of a vortex beam during propagation is effectively overcome, the generators may have potential applications for optical fiber optical wrench, all-fiber stimulated emission depletion microscopy, or orbital angular momentum fiber communication. Moreover, the compact generators also have a good anti-interference ability and long-term stability.

Vortex beams have attracted considerable interest in the past decades due to their unique and fascinating physical properties such as phase singularity, donut-shaped intensity pattern, and orbital angular momentum (OAM).[1–3] These properties of vortex beams have been used in a variety of application fields, including optical imaging,[4] optical communication,[5] and particle manipulation.[6] Previously, generating a vortex beam relies on free-space optical coupling, such as cylindrical-lens mode converters,[7] spatial light modulators,[8] microscopic ring resonators,[9] and spiral phase plates.[10] In the recent years, optical fiber-based vortex beam generation has attracted increasing attention, due to their compact size, low cost, and long-term environmental stability. Researchers have developed various all-fiber vortex beam generators fabricated from standard single-mode fibers,[11] few-mode fibers,[12,13] photonic crystal fibers,[14] and other special types of fibers,[15] which can be considered useful replacements of the conventional free-space vortex beam generators.

Generally, the vortex beam generated from these all-fiber generators is mainly based on the internal microstructure modulation inside the optical fiber. In practice, the optical fiber tip has also been demonstrated to be an inherently light-coupled microscopic platform for realizing various output light fields.[16,17] In the most recent years, fabricating photonic microstructures (such as a spiral phase plate or vortex grating) directly on the optical fiber tip creates opportunities for vortex beam generation,[18–20] although preparing micro–nano structures on an optical fiber tip is still very challenging.

Reviewing the previous research works, there are very few all-fiber optic components that are capable of generating a focused vortex beam directly. In fact, the intrinsically high divergence of a vortex beam during propagation may not be preferred in many practical applications such as the vortex beam coupling and particle manipulation. Instead of introducing a bulky element to focus the vortex beam from the fiber, in this paper, we report a compact all-fiber focused vortex beam generator, where a spiral zone plate (SZP) is integrated on top of an optical fiber using the femtosecond laser two-photon polymerization technology.

An SZP is an important type of a diffractive optical element that can be used to generate and focus a vortex beam in a single step.[21] A continuous-phase SZP is a combination of a spiral phase plate and

Fresnel zone plate, whose transmittance function can be expressed as follows:[22]

$$SZP_l(r,\varphi) = \exp\left(il\varphi - \frac{i\pi r^2}{\lambda f}\right), \quad (1)$$

where l is the topological number and represents the spiral arm number of the SZP, (r, φ) are the polar coordinates, and λ and f denote the designed wavelength and focal length, respectively. For a pure phase-type binarized SZP, all incident light is transmitted without loss, and the corresponding phase shift of π radians is transferred to the height of the polymer SZP zones using the following expression:

$$h = \frac{\lambda}{2(n_{SZP} - n_{medium})}, \quad (2)$$

where h is the total height of the SZP, and n_{medium} and n_{szp} are the refractive indexes of the surrounding medium (air) and SZP material polymerized from IP-L780 photoresist, respectively. In our work, the refractive index of the polymerized material was set to 1.48 for an operating wavelength of $\lambda = 1550$ nm, which was mainly based on the research results of Refs. 23 and 24. Figures 1(a)–1(c) show a schematic illustration of the SZP structure with different topological numbers ($l = 0$, 1, and 2), respectively.

Generally, fabricating the SZP on a standard single-mode fiber (SMF) tip is impractical for generating good focused vortex effects.

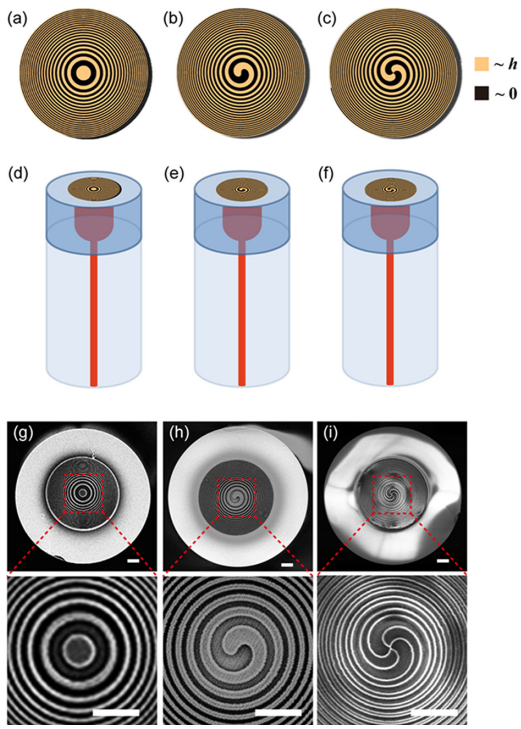

FIG. 1. [(a)–(c)] Schematic illustration of an SZP with topological number $l = 0$, 1, and 2. [(d)–(f)] Schematic of the focus vortex beam generators for $l = 0$, 1, and 2. [(g)–(i)] SEM images and the zoomed-in images of the microstructure for $l = 0$, 1, and 2 on the fiber tips, respectively. Scalebars in [(g)–(i)] are 10 μm.

Because the mode field diameter in an SMF is only a few micrometers, which inhibits vortex generation and focusing modulation ability. In our work, therefore, a standard SMF-28 (8.2/125 μm, YOFC) with 1 m length was first spliced to a segment of graded-index multimode fiber (62.5/125 μm, YOFC) using a fusion splicer (Fujikura 80S) after removing the exterior coating. Then, the multimode fiber was cut to a quarter-pitch length (245 $\pm$ 0.1 μm) with a computer-controlled precision cleaving system comprising an optical fiber cleaver, a precision translation stage with a step of 0.1 μm, and an industrial CCD camera.[11] Such a custom-mode fiber structure allows the Gaussian fundamental mode that propagates in the SMF to expand and collimate in the graded-index multimode fiber segment.

A cylindrical baseplate and SZP on the graded-index multimode fiber tips were written with a microfabrication system (Photonic Professional GT, Nanoscribe GmbH),[25] which takes advantage of the femtosecond laser two-photon polymerization technology.[26,27] The cylindrical baseplate with a diameter of 70 μm and a thickness of 5 μm was prepared to ensure the SZP can be firmly adhered to the end facet of the graded-index multimode fiber. The SZP was prepared to operate at $\lambda = 1550$ nm with a designed focal length of $f = 20$ μm on the cylindrical baseplate. The SZP diameter was designed to be 69 μm, which is slightly smaller than the size of the cylindrical baseplate. Finally, the focus vortex beam generators are designed, as shown in Figs. 1(d)–1(f), which correspond to topological charges $l = 0$, 1, and 2, respectively. Figures 1(g)–1(i) show scanning electron microscope images of the fabricated microstructures on the fiber tips.

Figure 2 shows a schematic diagram of the microfabrication system, where the writing light emitted from the laser first passed through a galvanometer scanning (x_g, y_g) system and was subsequently focused onto the IP-L780 photoresist with an oil immersion objective (Carl Zeiss, 63×, NA = 1.4). The optical fiber was fixed with a homemade fiber holder, which allows one to adjust the distance between the fiber facet and the thin microscope coverslip with a micrometer precision. The thickness of the microscope coverslip was 170 μm, and its upper and lower surfaces were deposited using the IP-L780 photoresist and optical index matching oil, respectively.

To characterize the vortex focusing behavior of the fabricated sample, we constructed a microscopic imaging system that uses a

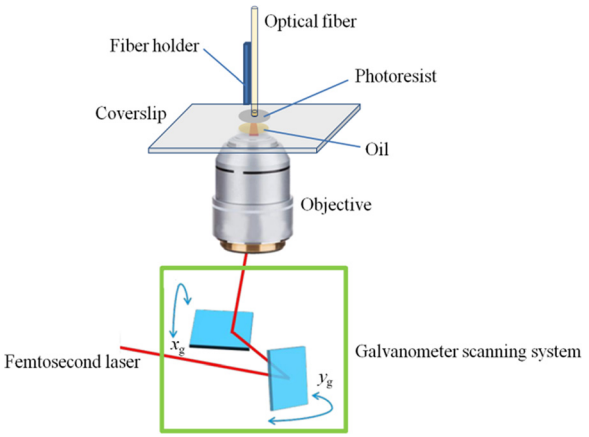

FIG. 2. Schematic of the SZP fabrication on the fiber tip using the femtosecond laser two-photon polymerization technology.

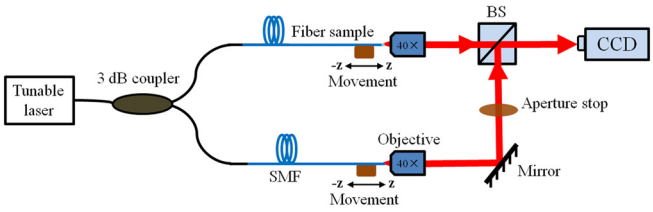

FIG. 3. Dual-beam interference microscopic imaging system.

dual-beam interference, as shown in Fig. 3. A tunable laser source (Agilent, Model 81940A) of which the wavelength was set to1550 nm was connected to a 3 dB coupler and then divided into two branch beams. One beam was coupled to the fabricated sample to generate a focused vortex beam, and the other branch was used as a reference beam to form a stable interference pattern with the former branch beam. As seen in Fig. 3, the virgin end of the fabricated fiber sample and the front end of an equal length standard SMF-28 were connected to the two outputs of the 3 dB coupler using a bare fiber adapter. The rear ends were fixed on a micromanipulation stage, which could be moved horizontally with high precision. The output beams from the fiber sample and SMF branches were magnified with a 40× objective lens. A beam splitter (BS) was placed at the point where the two magnified beams intersected, and the coaxial and non-coaxial interference patterns formed by the two beams were observed using an infrared CCD camera. Furthermore, when the reference beam was blocked with an aperture stop, the infrared CCD camera could only receive the intensity distribution of the out-coupled beam from the fiber sample.

The intensity distribution near the focus of the out-coupled beam was measured by blocking the reference beam. Each fiber sample with a different topological number ($l = 0$, 1, and 2) was moved horizontally from left to right in 5 μm sampling intervals by adjusting the micromanipulation stage. The measurement results are shown in Fig. 4, where the best focus position of the out-coupled light from the fiber sample was selected as the origin position. As can be seen in Fig. 4, the out-coupled light from different fiber samples could be focused to a very small spot. The difference is that when $l = 0$, the focus spot at the origin position exhibits a conventional point-like profile. However, the focus at the origin position exhibits a doughnut-shaped profile when $l \neq 0$. SZP structures with different topological charge numbers were clearly imaged with the infrared CCD camera as each fiber sample was moved toward the objective lens. The distance between the origin position and the special position, where the SZP contour could be clearly imaged, can be considered the actual focal length of the fiber sample. As seen from the last column in Fig. 4, the actual focal lengths for fiber samples with topological charges $l = 0$, 1, and 2 are 16.6, 15.8, and 15.4 μm, respectively. In addition, it is worth mentioning that the bending change of the SMF hardly causes any change in the diameter and shape of the focus spot. In other words, the all-fiber focused vortex beam generators can maintain a good resistance to bending interference.

Propagation of the out-coupled light from the fabricated fiber sample was simulated using the finite-difference time-domain (FDTD) method. The total intensity cross sections in the longitudinal plane (x, z) for $l = 0$, 1, and 2 can be clearly seen in Figs. 5(a)–5(c), respectively. As is illustrated in Fig. 5(a), when $l = 0$, the out-coupled light from the fiber sample was focused onto a single-lobe shape along the axial (z) direction. However, when $l = 1$ or 2, the out-coupled light is focused onto a dual-lobe shape, and the spacing between the two lobes increases gradually as the topological charge l increases, as shown in Figs. 5(b) and 5(c). The focal length was calculated to be 16.2, 15.4, and 15.1 μm for $l = 0$, 1, and 2, respectively. After comparing the focal length data shown in the last column of Fig. 4, we find that there is only a small numerical error between the calculated results and the measured results. It is worth noting that there is a large discrepancy between the designed focal length ($f = 20$ μm) and these calculated (or measured) focal lengths, which may be due to diffraction of the evanescent fields inside the subwavelength features of the SZP.[28]

Figures 5(d)–5(f) show the simulated intensity cross sections in the focal plane (x, y). The simulation results show that the light out-coupled from the fiber sample focuses to a solid dot spot when $l = 0$, while the focused beam is doughnut-shaped when $l = 1$ or 2. The calculated diameters of the focused spot are 2.36, 4.30, and 5.45 μm for $l = 0$, 1, and 2, respectively. Moreover, the focused spot size will continue to increase as the topological charge increases, which is verified with further simulations. In addition, we notice the broken axial

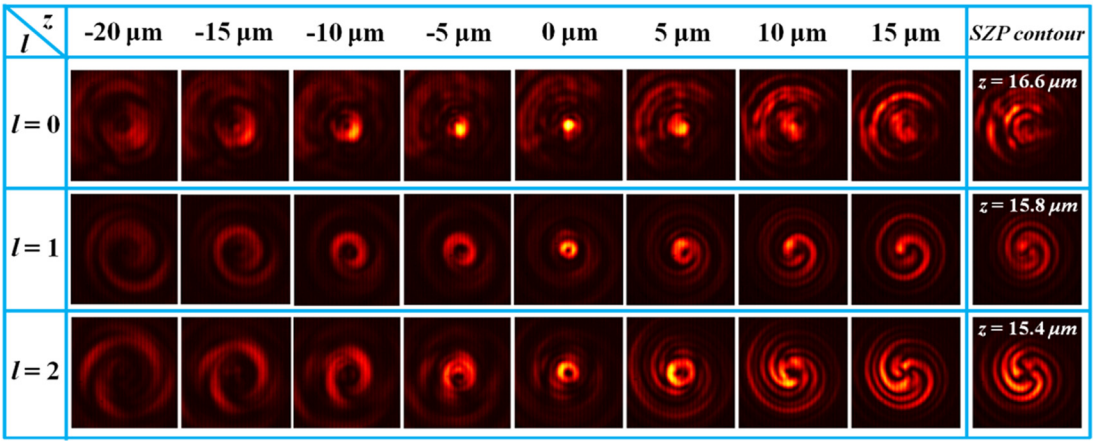

FIG. 4. Intensity distributions near the focus position of the out-coupled light from the fiber sample.

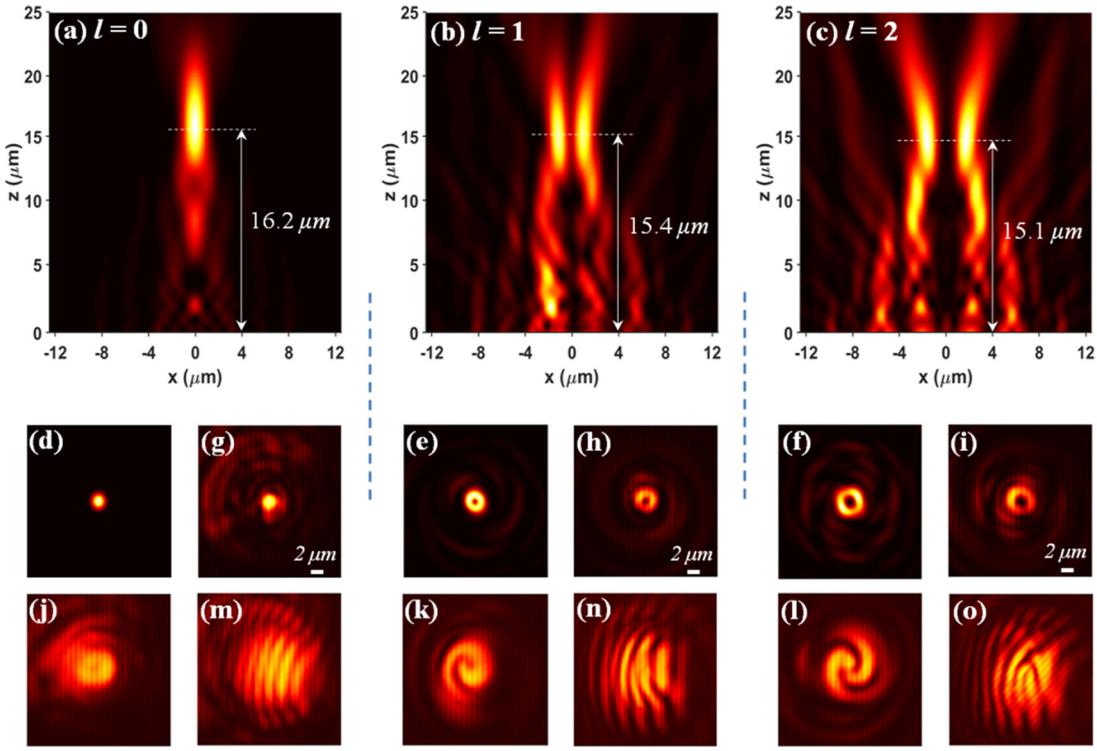

FIG. 5. [(a)–(c)] FDTD simulated intensity cross sections in the longitudinal plane (x, z) for $l = 0$, 1, and 2. [(d)–(f) and (g)–(i)] The intensity cross section in the focal plane (x, y) by FDTD simulation and experimental measurement, respectively. [(j)–(l) and (m)–(o)] Experimentally measured coaxial and non-coaxial interference patterns between the focus vortex beam and the Gaussian fundamental mode reference beam, respectively.

symmetry of the intensity pattern in the focused spots, especially when $l = 2$. The asymmetry can be primarily attributed to fabrication imperfections, the finite effective size, and the non-circular symmetry of the SZP structures.[21] All these simulated focus spots were measured in experiments, as seen in Figs. 5(g)–5(i). The measured focused spot diameters were 2.42, 4.33, and 5.52 μm for $l = 0$, 1, and 2, respectively, which are basically consistent with their corresponding numerical results.

The topological charges of the focused vortex beams were determined experimentally from coaxial and non-coaxial interferences with a Gaussian reference beam in the fundamental mode. As seen from Fig. 5(j), when $l = 0$, a coaxial interferogram exhibits a Newton-ring-like fringe pattern, which shows that the focused beam from the fiber sample does not carry any OAM. When $l = 1$ and 2, the coaxial interferogram clearly exhibits one-arm and two-arm spiraling interference patterns, respectively, as shown in Figs. 5(k)–5(l). The presence of the spiral arm in the interferograms shows that the focused out-coupled beam carries OAM. Moreover, the number of spiral arms is equal to the topological charge of the focused vortex beam. Similarly, Figs. 5(m)–5(o) show the non-coaxial interferograms. One can see that all non-coaxial interferograms exhibit fringe-shaped patterns. The main difference is that when $l = 0$, the interference forms a conventional comb-like fringe pattern, whereas when $l = 1$ and 2, the interference forms special fork-shaped fringe patterns. Moreover, the number of forks increases as l increases. The fork-shaped fringe once again confirms that the focused out-coupled light from the fiber sample carries OAM.

In summary, we presented a compact all-fiber focused vortex beam generator by integrating SZPs with different topological charge numbers on the top of optical fibers. Power throughputs of over 90% can be obtained for all focused vortex beam generators used in our experiments. Most of the power losses can be attributed to scattering and absorption in the cylindrical photopolymer baseplate and SZP structure. We can easily realize a precise manipulation of the output light field by changing the design parameters of the SZP integrated on the fiber tips. Furthermore, through several repeated experiments in two months, we found that the fabricated fiber samples have a good long-term stability. The proposed focused vortex beam generators may have important applications in optical fiber tweezers, optical fiber imaging, and optical fiber communication.

This work was financed by the National Natural Science Foundation of China (NSFC) (Nos. 61875134, 61425007, 61935013, and 61975133), the Science and Technology Innovation Commission of Shenzhen (Nos. KQJSCX20170727101953680, JCYJ20180507182058432, JCYJ20160427104925452, and JCYJ20180507182035270), the Natural Science Foundation of Guangdong Province Grant No. 2020A1515011185, the Development and Reform Commission of Shenzhen Municipality Foundation, and the China Postdoctoral Science Foundation (No. 2018M640816).

DATA AVAILABILITY

The data that support the findings of this study are available from the corresponding author upon reasonable request.

REFERENCES

[1]M. J. Padgett, Opt. Express **25**, 11265–11274 (2017).
[2]M. Padgett, J. Courtial, and L. Allen, Phys. Today **57**(5), 35–40 (2004).
[3]N. R. Heckenberg, R. McDuff, C. P. Smith, and A. G. White, Opt. Lett. **17**, 221–223 (1992).
[4]G. A. Swartzlander, Opt. Lett. **26**, 497–499 (2001).
[5]L. Liu, Y. Gao, and X. Liu, Opti. Commun. **452**, 40–47 (2019).
[6]M. Padgett and R. Bowman, Nat. Photonics **5**, 343–348 (2011).
[7]M. J. Padgett and L. Allen, J. Opt. B **4**, S17–S19 (2002).
[8]P. Gregg, P. Kristensen, and S. Ramachandran, Optica **2**, 267–270 (2015).
[9]X. Cai, J. Wang, M. J. Strain, B. Johnson-Morris, J. Zhu, M. Sorel, J. L. O'Brien, M. G. Thompson, and S. Yu, Science **338**, 363–366 (2012).
[10]P. Schemmel, G. Pisano, and B. Maffei, Opt. Express **22**, 14712–14726 (2014).
[11]C. Fu, S. Liu, Z. Bai, J. He, C. Liao, Y. Wang, Z. Li, Y. Zhang, K. Yang, B. Yu, and Y. Wang, J. Lightwave Technol. **36**, 1683–1688 (2018).
[12]Y. Zhao, Y. Liu, C. Zhang, L. Zhang, G. Zheng, C. Mou, J. Wen, and T. Wang, Opt. Lett. **42**, 4708–4711 (2017).
[13]G. Yin, C. Liang, I. P. Ikechukwu, M. Deng, L. Shi, Q. Fu, T. Zhu, and L. Zhang, Opt. Lett. **44**, 999–1002 (2019).
[14]C. Fu, S. Liu, Y. Wang, Z. Bai, J. He, C. Liao, Y. Zhang, F. Zhang, B. Yu, S. Gao, Z. Li, and Y. Wang, Opt. Lett. **43**, 1786–1789 (2018).
[15]Z. Bai, M. Li, Y. Wang, J. Tang, Z. Zhang, S. Liu, C. Fu, Y. Zhang, J. He, Y. Wang, and C. Liao, Appl. Phys. Express **12**, 072004 (2019).
[16]E. Brasselet, M. Malinauskas, A. Žukauskas, and S. Juodkazis, Appl. Phys. Lett. **97**, 211108 (2010).
[17]M. Malinauskas, A. Žukauskas, V. Purlys, K. Belazaras, A. Momot, D. Paipulas, R. Gadonas, A. Piskarskas, H. Gilbergs, A. Gaidukevičiūtė, I. Sakellari, M. Farsari, and S. Juodkazis, J. Opt. **12**, 124010 (2010).
[18]K. Weber, F. Huett, S. Thiele, T. Gissibl, A. Herkommer, and H. Giessen, Opt. Express **25**, 19672–19679 (2017).
[19]P. Vayalamkuzhi, S. Bhattacharay, U. Eigenthaler, K. Keskinbora, C. T. Samlan, M. Hirscher, J. P. Spatz, and N. K. Viswanathan, Opt. Lett. **41**, 2133–2136 (2016).
[20]Z. Xie, S. Gao, T. Lei, S. Feng, Y. Zhang, F. Li, J. Zhang, Z. Li, and X. Yuan, Photonics Res. **6**, 743–749 (2018).
[21]A. Balcytis, D. Hakobyan, M. Gabalis, A. Zukauskas, D. Urbonas, M. Malinauskas, R. Petruskevicius, E. Brasselet, and S. Juodkazis, Opt. Express **24**, 16988–16998 (2016).
[22]Z.-N. Tian, Q.-D. Chen, Z.-Y. Hu, Y.-K. Sun, Y.-H. Yu, H. Xia, and H.-B. Sun, Opt. Lett. **43**, 3116–3119 (2018).
[23]T. Gissibl, S. Wagner, J. Sykora, M. Schmid, and H. Giessen, Opt. Mater. Express **7**, 2293–2298 (2017).
[24]Y. Li, S. Park, M. Mclamb, M. Lata, S. Schöche, D. Childers, I. D. Aggarwal, M. K. Poutous, G. Boreman, and T. Hofmann, Opt. Mater. Express **9**, 4318–4328 (2019).
[25]See https://www.nanoscribe.com/en/solutions/materials for the microfabrication system (Photonic Professional GT, Nanoscribe GmbH).
[26]Z. Li, C. Liao, J. Wang, Z. Li, P. Zhou, Y. Wang, and Y. Wang, J. Lightwave Technol. **37**, 1241–1245 (2019).
[27]L. Jonušauskas, D. Gailevičius, S. Rekštytė, T. Baldacchini, S. Juodkazis, and M. Malinauskas, Opt. Express **27**(11), 15205–15221 (2019).
[28]H. J. Lezec and T. Thio, Opt. Express **12**, 3629–3651 (2004).